

# Journal of Biomedical Optics

[SPIEDigitalLibrary.org/jbo](http://SPIEDigitalLibrary.org/jbo)

## **Differential diagnosis of nonmelanoma pigmented skin lesions based on harmonic generation microscopy**

Ming-Rung Tsai  
Yu-Hsiang Cheng  
Jau-Shiuh Chen  
Yi-Shuan Sheen  
Yi-Hua Liao  
Chi-Kuang Sun

# Differential diagnosis of nonmelanoma pigmented skin lesions based on harmonic generation microscopy

Ming-Rung Tsai,<sup>a,b</sup> Yu-Hsiang Cheng,<sup>a</sup> Jau-Shiuh Chen,<sup>c</sup> Yi-Shuan Sheen,<sup>c</sup> Yi-Hua Liao,<sup>b,c,\*</sup> and Chi-Kuang Sun<sup>a,b,d,e,\*</sup>

<sup>a</sup>National Taiwan University, Graduate Institute of Photonics and Optoelectronics and Department of Electrical Engineering, Taipei 10617, Taiwan

<sup>b</sup>National Taiwan University, Molecular Imaging Center, Taipei 10617, Taiwan

<sup>c</sup>National Taiwan University Hospital and National Taiwan University College of Medicine, Department of Dermatology, Taipei 10002, Taiwan

<sup>d</sup>Research Center for Applied Sciences and Institute of Physics, Academia Sinica, Taipei 11529, Taiwan

<sup>e</sup>National Taiwan University, Graduate Institute of Biomedical Electronics and Bioinformatics, Taipei 10617, Taiwan

**Abstract.** *In vivo* harmonic generation microscopy (HGM) has been applied successfully in healthy human skin and can achieve a submicron resolution, similar to histopathologic examination, even at a penetration depth up to 270  $\mu\text{m}$ . This study aims to investigate the clinical applicability of HGM imaging for differential diagnosis of nonmelanoma pigmented skin lesions. A total of 42 pigmented skin tumors, including pigmented basal cell carcinoma, melanocytic nevus, and seborrheic keratosis were evaluated by HGM *ex vivo* or *in vivo*. Based on the standard histopathologic characteristics, we established the corresponding HGM imaging criteria for each pigmented tumor. Diagnostic performance of HGM for differentiating nonmelanoma pigmented skin tumors was evaluated through the observers' direct general assessment (overall evaluation) or the presence of two imaging criteria with the highest sensitivity and specificity (major criteria evaluation). Our results show that, based on the direct general assessment, the sensitivity is 92% [95% confidence interval (CI): 67 to 97%] and the specificity is 96% (95% CI: 83 to 99%); by major criteria evaluation, 94% sensitivity (95% CI: 70 to 99%) and 100% specificity (95% CI: 87 to 100%) are achieved. Our study indicates that HGM serves as a promising histopathological examination tool for noninvasive differential diagnostics of nonmelanoma pigmented skin tumors. © The Authors. Published by SPIE under a Creative Commons Attribution 3.0 Unported License. Distribution or reproduction of this work in whole or in part requires full attribution of the original publication, including its DOI. [DOI: 10.1117/1.JBO.19.3.036001]

Keywords: diagnosis; basal cell carcinoma; melanocytic nevi; seborrheic keratosis; harmonic generation microscopy.

Paper 130604PRR received Aug. 19, 2013; revised manuscript received Jan. 14, 2014; accepted for publication Jan. 28, 2014; published online Mar. 3, 2014.

## 1 Introduction

Because of the increasing prevalence of skin cancer, screening for malignant skin lesions has become a common prevention intervention for the general population. Among skin cancers, basal cell carcinoma (BCC) is a common skin cancer accounting for a dominant part of all skin cancers worldwide.<sup>1</sup> In Asians, the BCC, which typically presents as pigmented skin lesions with a rolled pearly border and telangiectasia,<sup>1,2</sup> is the most common skin cancer, accounting for ~70% of all malignant cutaneous tumors.<sup>1,2</sup> Although it rarely metastasizes, BCC can cause significant destruction and disfigurement by local invasion.<sup>3</sup> Melanocytic nevus and seborrheic keratosis (SK) are the two most common benign pigmented skin lesions that, importantly, may mimic BCC clinically.<sup>4,5</sup> Patients are often worried about the change in appearance of their pigmented skin lesions and concerned about the potential of the lesions to turn into a skin malignancy. Given the large variation of the appearance and behavior of pigmented skin tumors, diagnosis by the naked eye is certainly insufficient to identify skin cancers.<sup>5,6</sup> Therefore, the timely and precise detection of malignant pigmented tumors is strongly required to ease patient anxiety and improve clinical outcomes.

Dermoscopy has been proven to provide the pattern of pigment in diagnosing pigmented skin tumors,<sup>7-9</sup> but it cannot provide histopathological features to make a final diagnosis. Therefore, skin biopsy with histopathological examination is still the standard diagnostic method for skin cancer. The procedure of biopsy, which requires removal, fixation, embedding, sectioning, and staining of lesional skin tissues, is labor-intensive, time-consuming, and may involve unwanted processing artifacts. Skin biopsy is also invasive and can cause discomfort to the patients. It is, thus, desirable to develop noninvasive imaging tools capable of providing histopathological information. The need for providing noninvasive methods for diagnosing skin tumors has led to the development and investigation of a variety of imaging tools, such as high-resolution ultrasound,<sup>10</sup> optical coherence microscopy,<sup>11</sup> confocal microscopy,<sup>12-15</sup> two-photon fluorescence microscopy,<sup>16-18</sup> and harmonic generation microscopy (HGM), which includes second-harmonic-generation (SHG) and third-harmonic-generation (THG) imaging modalities.<sup>19</sup>

Similar to two-photon fluorescence microscopy based on a Ti:sapphire laser, which has been frequently combined with the SHG modality for exploration of skin lesions,<sup>16-18,20-22</sup> HGM is based on nonlinear optical processes to provide high three-dimensional resolution. Different from the two-photon fluorescence process, higher harmonic generation processes mostly excited with an ~1230 nm pulsed Cr:forsterite laser are

\*Address all correspondence to: Yi-Hua Liao and Chi-Kuang Sun, E-mail: yihualiao@ntu.edu.tw and sun@ntu.edu.tw

based on virtual transitions. Without electronic transitions, higher-harmonic-generation processes are known to leave no energy deposition to the interacted tissues, and therefore, no photodamage and photobleaching effects are observed.<sup>23–25</sup> A recent study reported that the SHG images excited by a Ti:sapphire laser with a wavelength of 800 nm became out of focus when the probing depth exceeded 110  $\mu\text{m}$ , and the SHG light almost disappeared beyond a depth of 200  $\mu\text{m}$ .<sup>26</sup> However, under the same excitation power while utilizing a Cr:forsterite laser as the excitation source, the SHG images became out of focus and lost sharpness beyond a 250- $\mu\text{m}$  depth, and the SHG signals were still detectable even at a depth of 350  $\mu\text{m}$ .<sup>26</sup> In addition to the penetration depth, the noninvasiveness is also an important issue for *in vivo* applications. In our previous mouse embryo study, by using an excitation laser at 1230 nm, a similar rate of blastocyst development could be found in imaged embryos versus nonimaged control set under the average power of 140 mW.<sup>27</sup> Under the excitation wavelengths of 730 to 800 nm, the common laser sources used in two-photon fluorescence technique, hamster ovary cells were found to be unable to form clones with >6 mW mean power, and complete cell destruction occurred at an average power >10 mW.<sup>28</sup> Moreover, it has been shown that the formation of cyclobutane pyrimidine dimers in cellular DNA was induced under the two-photon process at the excitation wavelengths of 695 to 810 nm.<sup>29</sup>

HGM has been demonstrated to have a superior performance on healthy human skin, in terms of submicron resolution, cellular contrast provision, penetration capability, and noninvasiveness.<sup>19,30,31</sup> A previous HGM study revealed its excellent imaging capability to directly provide histopathological information for differentiation of oral cancerous tissues from normal mucosa.<sup>32</sup> Furthermore, we found that melanin pigment provides a strong source of THG contrast.<sup>19</sup> These results underline the potential applicability of the 1230-nm-based HGM for noninvasive, *in vivo* histopathological diagnosis of pigmented skin tumors. The goal of this study is to establish HGM diagnostic criteria for three most commonly occurring nonmelanoma pigmented skin lesions, melanocytic nevus, SK, and BCC, and to evaluate the applicability of HGM for their differential diagnosis.

## 2 Materials and Methods

### 2.1 Subjects

In this study, the inclusion criteria were patients aged 18 to 90 years and having pigmented skin lesions that would undergo surgical excision. The patients who had infectious skin disease on the examination sites were excluded. HGM was performed *ex vivo* on surgical samples and *in vivo* directly on the lesional skin before surgical excision. After HGM observation, all surgically removed specimens were sent for histopathological analysis to confirm the diagnosis. Among them, there were 47 nonmelanoma pigmented lesions, but HGM image acquisition from five *in vivo* lesions (two melanocytic nevi, two BCC, and one SK) could not be completed because of an overlying thick horny layer (e.g., nail and palm) or lesions being located on areas with irregular curvature that the objective lens could not closely approach (e.g., the nasal bridge). HGM images of 42 nonmelanoma pigmented lesions (14 *ex vivo* and 28 *in vivo*) from 40 patients (24 men and 16 women, age range of 23 to 82; two patients had two lesions), which included 18 melanocytic

nevi (2 *ex vivo* and 16 *in vivo*), 10 SK (2 *ex vivo* and 8 *in vivo*), and 14 pigmented BCC (10 *ex vivo* and 4 *in vivo*; nodular and superficial types), were evaluated in this study. The process of image acquisition was performed under the protocol reviewed and approved by the Research Ethics Committee of National Taiwan University Hospital. Informed consent was obtained from each subject prior to study entry.

### 2.2 Harmonic Generation Microscopy

The HGM system was modified from a commercial scanning system (Olympus, FV300) and was excited by a Cr:forsterite laser with a wavelength of 1230 nm, a pulse width of 100 fs, a repetition rate of 110 MHz, and an output average power of 500 mW. This excitation wavelength enables minimal light attenuation in skin and mucosa tissues.<sup>33</sup> Figure 1 is the schematic diagram of the HGM imaging system. The collimated laser beam transmitted through the scanning system, an 865-nm dichroic beam splitter (DBS1), and an infrared water immersion objective (Olympus, UPlanApo/60 $\times$ /NA = 1.2) to excite skin or skin samples. The backward harmonic generation signals were collected by the same objective and reflected by DBS1 to two photomultiplier tubes (Harmamatsu R4220P for THG and Harmamatsu R928P for SHG). SHG and THG signals were divided by a 490-nm dichroic beam splitter (DBS2) and were filtered by two bandpass filters (D410/30 for THG and D615/10 for SHG) inserted. Based on the Cr:forsterite laser at 1230 nm, our previous HGM studies have indicated a diminished two-photon fluorescence in viable epidermis and dermis by measuring the spectra in live human skin.<sup>23,34,35</sup> Submicron spatial resolution could be achieved (lateral <0.5  $\mu\text{m}$  in superficial layers and <0.7  $\mu\text{m}$  at a 270  $\mu\text{m}$  depth) for THG, which is the primary contrast modality for cancer diagnosis in this study. The total exposure time of the laser light for one volunteer was equal to or slightly less than 30 min. The average excitation power after the objective was around but slightly less than 100 mW. The accumulated photon energy was  $\sim$ 180 J in each volunteer. Under such an accumulated light dose, no erythema, pigmentation, or blister formation on the examined skin was found in this study. For all followed-up histological examinations by pathologists on the illuminated specimens, no evidence of photodamage, such as coagulation necrosis, was found.

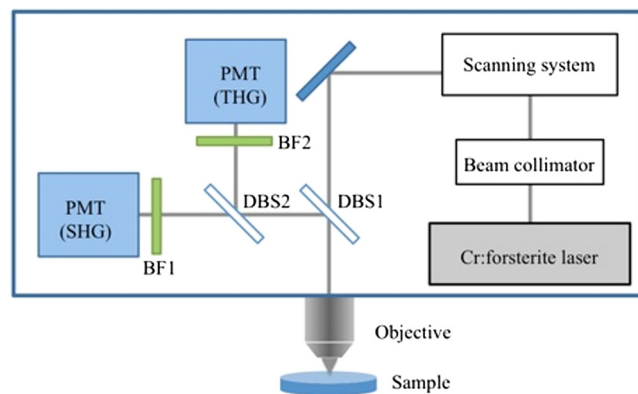


**Fig. 1** Harmonic generation microscopy imaging system. The illumination source was a Cr:forsterite laser. The collimated laser beam performed a scanning system. Second-harmonic-generation and third-harmonic-generation (THG) signals were divided by a dichroic beam splitter and guided to two photomultiplier tubes with bandpass filters inserted.

### 2.3 HGM Feature Description

Under THG images, the cell nuclei appear dark and the cytoplasm of cells appear bright. The proliferation of cells means an increase in cell number. According to the uniformity of cellular size and morphology, the proliferation of THG-bright cells with bright cytoplasm and dark nucleus in the stratum granulosum and spinosum was defined as monomorphous or polymorphous cells. The cell nests in rete ridges or in the dermis were also recognized as two types, namely monomorphous and polymorphous cell nests. Elongation of rete ridges represented the presence of rete ridges that could be observed continuously for a depth beyond 50  $\mu\text{m}$ . Normal epidermal stratification indicated that the stratum corneum, granulosum, and spinosum could be visualized clearly in serial optical sections. Acanthotic epidermis meant that the thickness of epidermis was increased compared to the surrounding normal skin. Changes in connective tissues represented altered distribution or density of SHG-bright collagen fibers.

### 2.4 Image Analysis and Statistics

The database of HGM images from 42 nonmelanoma pigmented tumors was retrospectively analyzed by three independent observers in a blinded fashion (blinded to participant name, sex, age, and diagnosis). One week before the assessment, the observers were instructed in the interpretation of the *en face* HGM images using representative images for each HGM criterion. During the assessment, the presence or absence of the HGM criteria (Table 1) was documented, and a tentative diagnosis was given under observer's general assessment for individual case. The HGM data were compared with the

**Table 1** Sensitivity and specificity of individual harmonic generation microscopy (HGM) diagnostic criterion.

Disease diagnostic criteria	Sensitivity (95% CI)	Specificity (95% CI)
Basal cell carcinoma ( $n = 14$ )		
Peripheral palisading cells	95 (84 to 99)	100 (96 to 100)
Proliferation of polymorphous basaloid cells	98 (88 to 100)	90 (82 to 95)
Elongated cells/nuclei	88 (75 to 95)	92 (85 to 96)
Collagen changes	67 (52 to 79)	98 (92 to 99)
Melanocytic nevus ( $n = 18$ )		
Monomorphous cell nests	98 (90 to 100)	96 (89 to 99)
Normal epidermal stratification	98 (90 to 100)	88 (80 to 94)
Elongation of rete ridges	74 (61 to 84)	81 (71 to 88)
Seborrheic keratosis ( $n = 10$ )		
Proliferation of monomorphous basaloid cells	97 (83 to 99)	98 (93 to 99)
Acanthotic epidermis	97 (83 to 99)	100 (96 to 100)

Note: CI, confidence interval.

histopathological findings that were exploited as the gold standard. Sensitivity and specificity analysis was performed with cross-tabulations and SPSS 12.0 software (SPSS Inc., Chicago, Illinois). Calculations were carried out for each criterion alone and in combination with two major criteria.

## 3 Results

### 3.1 HGM Images of Healthy Skin

Morphologic information of normal skin was assessed *in vivo* according to our previous HGM studies.<sup>19,30,31</sup> As shown in Figs. 2(a) to 2(d), different cell morphologies and sizes can be visualized in optical sections taken at different depths parallel to the skin surface through THG images (presented by purple pseudocolor). Due to the multilayer structures of the stratum corneum and lipids within the corneocytes, the stratum corneum appeared bright with a strong contrast of THG [Fig. 2(a)]. As the imaging depth moved deeper into the viable epidermis [Figs. 2(b) to 2(d)], the stratum granulosum, spinosum, and

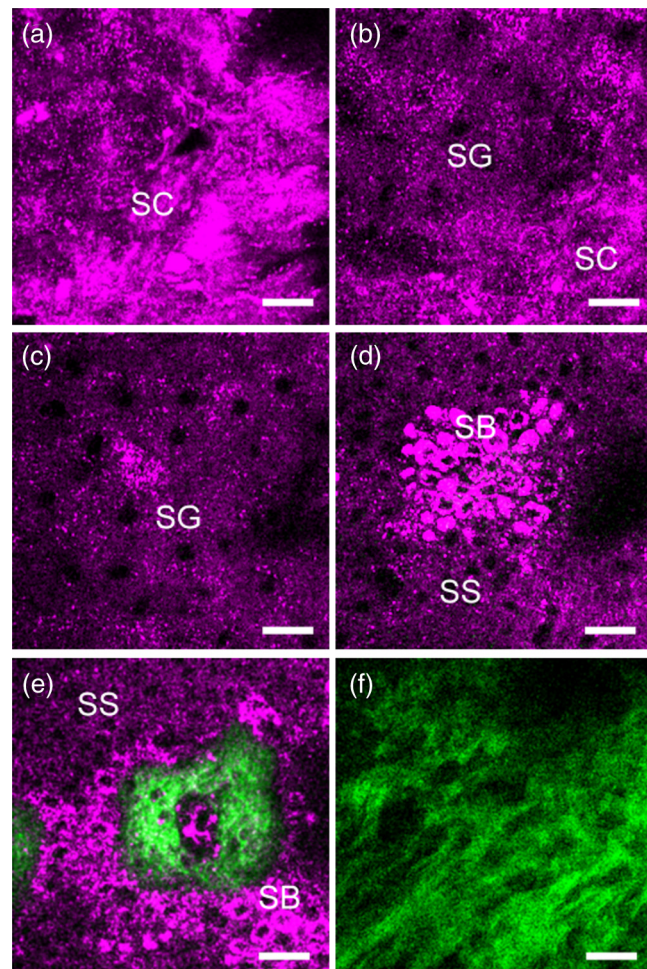


**Fig. 2** The harmonic generation microscopy (HGM) images of normal skin on arm. A representative *in vivo* series of horizontal HGM images from healthy skin at different depths relative to the surface (5, 15, 30, 45, 60, and 85  $\mu\text{m}$ ) showed different epidermal layers [(a) to (d)], the dermo-epidermal junction (e), and the dermis (f). SC, stratum corneum; SG, stratum granulosum; SS, stratum spinosum; SB, stratum basale. Bars = 20  $\mu\text{m}$ .

basale could be visualized showing cells with bright cytoplasm and dark nuclei. The sizes of basal cells are smaller than the cells in the spinous layer, and the cytoplasm of basal cells revealed strong THG contrasts owing to the resonance enhancement of melanin.<sup>19</sup> In addition to cell morphology, HGM provided the contrast of collagen fibers from SHG (presented by green pseudocolor) in the dermis [Fig. 2(f)]. Thus, the dermo-epidermal junction [Fig. 2(e)] could be explicitly observed by combining SHG and THG signals.

### 3.2 HGM Images of Melanocytic Nevus

Normal epidermal stratification beginning from the stratum corneum, granulosum to spinosum was observed. The presence of the aggregation of THG-bright cells in the dermo-epidermal junction [Fig. 3(a), dashed circle] and in the dermis [Fig. 3(c), arrows] was found in junctional and intradermal melanocytic nevus, respectively, in accordance with the nests of nevomelanocytes found by the conventional pathologic examination from the same tumors [Figs. 3(b) and 3(d)]. The cells in the nests were monomorphic in size and shape, and could be revealed from both THG imaging and the histopathologic examination. The THG-bright cells distributed linearly along the elongated rete ridges represented basal hyperpigmentation in junctional nevus. Some scattered melanocytes [Fig. 3(a), arrow], which had dendritic processes and were larger than basal cells, were also found in the stratum basale.

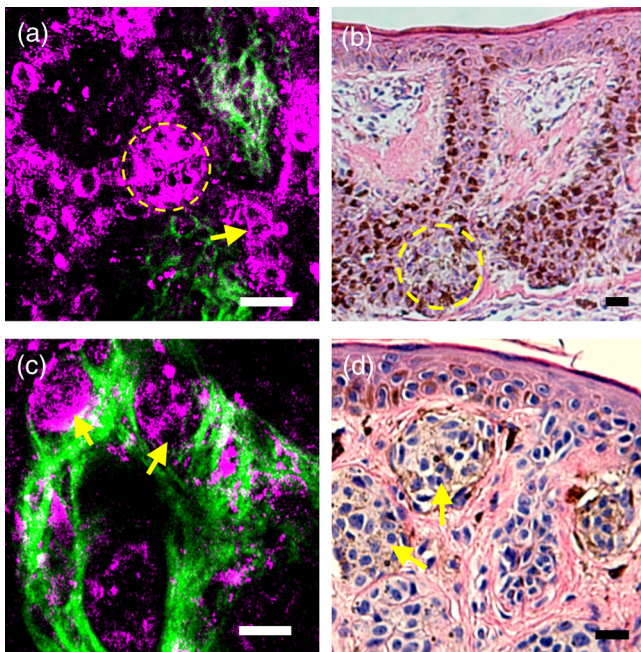


**Fig. 3** Representative *in vivo* HGM images of junctional nevus and intradermal nevus. (a) THG-bright monomorphic nevus cell nests (dashed circle) and scattered dendritic melanocytes (arrows) in the elongated rete ridges were observed in a junctional nevus. The junctional nests can be seen as a compact, well-outlined structure in contiguity with the basal layer. (c) Well-circumscribed, THG-bright monomorphic cell nests (arrows) in the dermis of an intradermal nevus. Comparative hematoxylin and eosin (H&E)-stained skin biopsy of the junctional nevus (b) and the intradermal nevus (d), respectively (vertical plane). Bars = 20  $\mu$ m.

### 3.3 HGM Images of Acanthotic Seborrheic Keratosis

The series of *in vivo* HGM images obtained from an acanthotic SK at different depths [Figs. 4(a) to 4(f)] showed the proliferation of THG-bright keratinocytes in the lower epidermis. Due to the increased melanin content, THG-bright cytoplasm was observed in some spinous cells and the majority of monomorphic basaloid cells [Fig. 4(c), arrows]. More epidermal HGM sections were taken in SK than that in normal skin, which indicated epidermal acanthosis. Intact dermo-epidermal junction with linearly aligned normal basal cells could be seen clearly [Fig. 4(f), arrows]. The corresponding histological section showed acanthotic epidermis and proliferation of melanin-containing basaloid cells [Fig. 4(g)].

### 3.4 HGM Images of Basal Cell Carcinoma

Many characteristic morphological abnormalities were present in BCC through *in vivo* HGM observations. There were THG-bright cell islands raising from the stratum basale and extending into the dermis [Figs. 5(d) to 5(f)]. These THG-bright cells appeared polymorphous with variation in size and shape. In contrast to the round to oval shapes of the normal basal cells with well-defined borders, many of the BCC cells became elongated with irregular borders. The presence of peripheral palisading cells in the tumor nodules was detected *in vivo* by HGM [Fig. 5(e), dashed line]. Collagen bundles surrounding the tumor nests [Fig. 5(e), dashed circle] in the reticular dermis became more thickened and coarse than the normal counterpart as revealed from SHG images [Fig. 5(e), yellow arrow]. The most striking finding was the presence of a large number of cells with dendritic processes [Figs. 5(f) and 5(g) to 5(i), arrows].

### 3.5 Sensitivity and Specificity of HGM Criteria

The images from 42 tumors were analyzed in an observer-blinded manner to evaluate the presence or absence of HGM diagnostic morphologic criteria, which were established according to the traditional histopathological features of BCC, melanocytic nevus, and SK. Using the corresponding pathologic examination of each lesion as the golden reference, Table 1 shows summaries of the sensitivity and specificity for each HGM diagnostic criterion. We selected two HGM criteria with the highest sensitivity and specificity as major criteria for each disease. Take BCC, for instance; the presence of polymorphous basaloid cells and cells with peripheral palisading were selected as major HGM criteria for diagnosing BCC because they were the two criteria with the highest sensitivity and specificity compared to the other two. As mentioned previously, the dendritic cell can be commonly found in BCC cases. We obtained the sensitivity and specificity of the dendritic cells as 95% (95% CI: 72 to 99%) and 89% (95% CI: 70 to 94%), respectively. As the presence of dendritic cells is not a diagnostic gold standard in pathology, this feature is not included in the statistics for diagnostic performance.

### 3.6 Sensitivity and Specificity of HGM for Diagnostic Performance

Our aim is to explore the clinical applicability of HGM by evaluating the diagnostic performance of HGM for differential diagnosis of nonmelanoma pigmented skin tumors. We

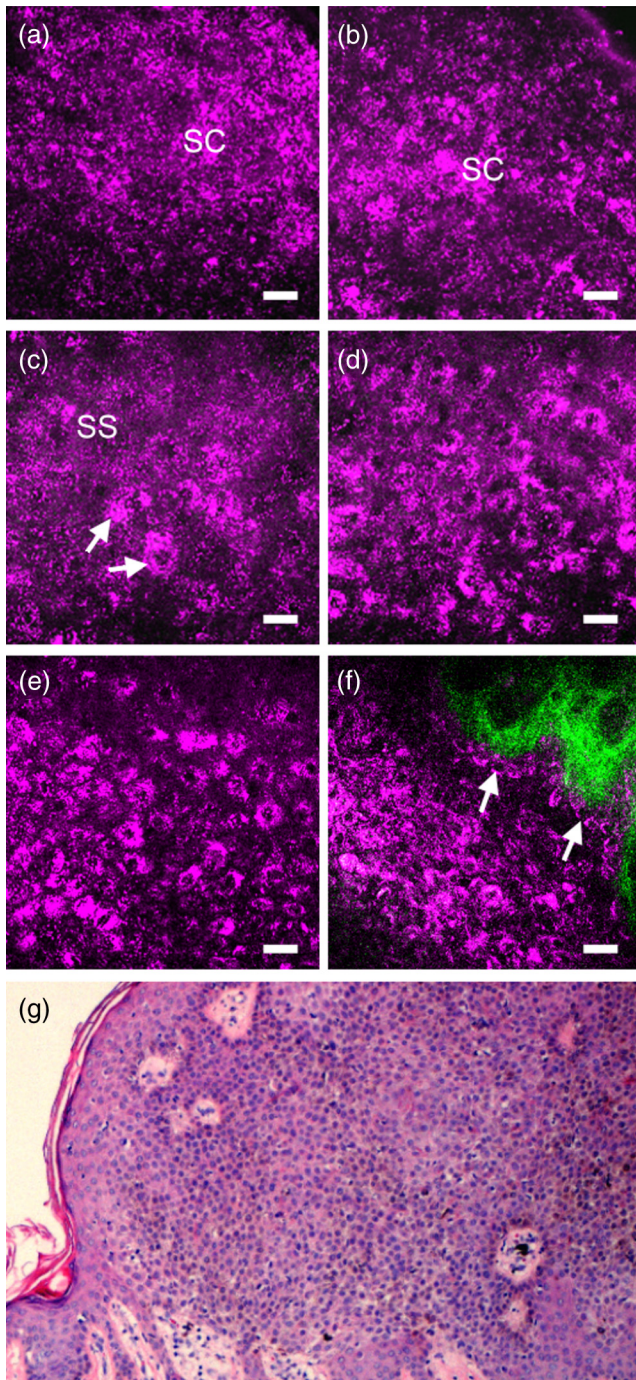


**Fig. 4** Acanthotic seborrheic keratosis. [(a) to (f)] A representative series of *in vivo* HGM images at different depths relative to the surface (5, 40, 65, 85, 105, and 130  $\mu\text{m}$ ). The whole thickness of the epidermis increased to  $\sim 130 \mu\text{m}$ . (a) and (b) Thickened stratum corneum ( $\sim 40 \mu\text{m}$ ) was observed, which correlated with the hyperkeratosis of seborrheic keratosis. (c) Scattered THG-bright spinous cells were noted (arrows), which resulted from melanin retention in the cytosol. (d) to (f) Proliferation of monomorphous THG-bright basaloid cells in the lower epidermis. The dermo-epidermal junction was intact with linearly aligned basal cells noted [arrows; (f)]. (g) H&E-stained section of the lesion. Bars = 20  $\mu\text{m}$ .

analyzed the diagnostic performance from 42 pigmented tumors through the direct general assessment (overall evaluation) or the presence of two imaging criteria (major criteria evaluation). In the overall evaluation, each specified HGM criterion was taken into account under the diagnostic decision

process, and the observers were asked to give the final diagnosis under general assessment. Based on a judgment process similar to the traditional pathological interpretation, 92% sensitivity (95% CI: 67 to 97%) and 96% specificity (95% CI: 83 to 99%) could be achieved (Table 2). In major criteria evaluation, which exploited the two specified criteria with the highest sensitivity and specificity for the diagnostic decision, 94% sensitivity (95% CI: 70 to 99%) and 100% specificity (95% CI: 87 to 100%) were achieved (Table 2). Taken together, excellent diagnostic performances with high sensitivity and specificity can be achieved through direct general assessment or the presence of two imaging criteria. These results indicate that HGM can provide real-time, accurate diagnostic outcomes. It is important to note that not all considered features are present in one lesion, which is true for our *in vivo* images and for traditional stained images. In addition, we also evaluated the performance of HGM for differential diagnosis in direct general assessment by comparing the *ex vivo* and the *in vivo* data. The sensitivities for *in vivo* data and *ex vivo* data were 92 and 99%, respectively. The specificity of 95% for *in vivo* data and 96% for *ex vivo* data could be obtained. There was no statistically significant difference in the diagnostic sensitivity as well as specificity between *ex vivo* and *in vivo* groups.

#### 4 Discussion

Although melanin pigment provides a strong source of THG contrast,<sup>19</sup> HGM imaging also revealed its excellent imaging capability to provide histopathological information in oral mucosa<sup>32,36</sup> and skin<sup>19,30,31</sup> without the presence of pigmentation. Due to the large variation of the appearance of pigmented skin tumors in clinical diagnosis, we focused on the differentiation of pigmented skin lesions in this study. Our results showed that the traditional histopathological features, such as monomorphous cell nests in nevocellular nevus, or peripheral palisading of tumor cells in BCC, could clearly be observed using HGM. Moreover, the sensitivity/specificity analysis demonstrated that HGM possessed excellent diagnostic performance, based on both the general assessment and major criteria assessment. Therefore, HGM is a promising, noninvasive *in vivo* imaging tool having a submicron resolution that opens a window into biotissues.

Cr:forsterite laser-based HGM has been demonstrated as a safe imaging device with no evidence of tissue damage based on a clinical trial of 52 healthy individuals.<sup>31</sup> In this study, after *in vivo* HGM measurements, the skin tumor was excised and processed for routine histological examination. We found no pathological evidence of photodamage, such as coagulation necrosis or subepidermal vesicular formation. Similarly, reflectance confocal microscopy using a low-power laser also provides a safe, *in vivo* modality for the examination of human skin.<sup>37</sup> However, multiphoton fluorescence microscopy using a femtosecond-pulsed near-infrared laser with the wavelength of 700 to 800 nm should cause concern about the risk of photodamage.<sup>38,39</sup> Therefore, with a richer contrast, a much improved spatial resolution, and an improved penetration capability compared to reflectance confocal microscopy, HGM offers the unique opportunity to investigate the skin with a high penetration depth, a subcellular spatial resolution, and a high safety profile at the same time. Compared with the healthy volunteers, in which HGM can achieve a penetration depth in skin of at least 300  $\mu\text{m}$ ,<sup>30</sup> in this study we found that HGM can also achieve a similar penetration depth ( $>270 \mu\text{m}$ ) in pigmented lesions

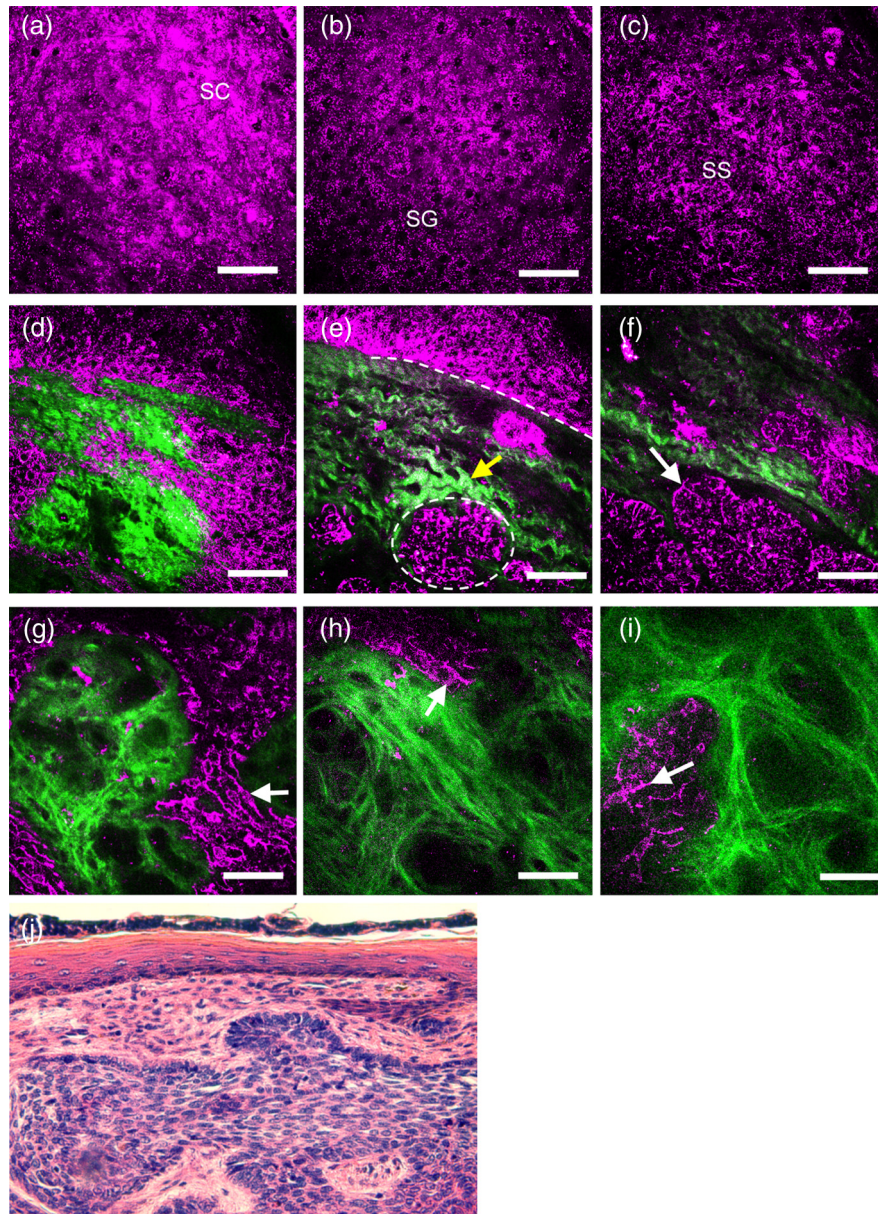


**Fig. 5** Basal cell carcinoma. (a) to (f) A representative series of *in vivo* HGM images of a case of basal cell carcinoma (BCC) at different depths relative to the surface (5, 25, 40, 60, 75, and 90  $\mu\text{m}$ ) revealed proliferation of polymorphous THG-bright tumor cells from the stratum basale (d) and continuously extended into the dermis [dashed circle; (e)] from one BCC patient. Several tumor nests [arrow; (f)] were found in the dermis. The tumor cells appeared irregular, elongated, and peripheral palisaded [dashed line; (e)]. Collagen bundles [yellow arrow; (e)] surrounding the tumor nests were more thickened and coarse than the normal counterpart. A characteristic feature noted was the presence of a large number of cells with dendritic processes [arrow; (f)], and the feature can also be found from the other patient with deeply invasive BCC at different depths relative to the surface (80, 150, and 270  $\mu\text{m}$ ) [arrows; (g) to (i)]. (j) H&E-stained section of the first lesion. SC, stratum corneum; SG, stratum granulosum; SS, stratum spinosum. Bars = 50  $\mu\text{m}$ .

*in vivo*, as shown in Fig. 5(i). This is due to the fact that in both healthy and lesion cases, the system penetration depths are both limited due to the working distance of the adopted objective.

Due to the subcellular resolution and the combined acquisition of SHG and THG signals of HGM, the histopathological features of individual nonmelanoma pigmented tumor could be revealed clearly to make the differential diagnosis successful. Our results suggest that the locations of cell nests and the

morphology of proliferating THG-bright cells were important for identifying a specific disease. For diagnosing BCC by HGM, we found that the peripheral palisading cells were able to provide significant diagnostic clues for BCC. In addition to the morphological abnormalities of tumor cells, the changes in peritumoral connective tissue can also be clearly revealed from SHG images. Furthermore, HGM provides excellent capability to clearly distinguish the epidermis and the dermis, which is crucial to reveal the degree of tumor invasion.

**Table 2** Sensitivity and specificity of HGM for differential diagnosis of nonmelanoma pigmented tumors.

	Sensitivity (95% CI)		Specificity (95% CI)	
	General assessment	Presence of two major criteria <sup>a</sup>	General assessment	Presence of two major criteria <sup>a</sup>
BCC	95 (72 to 99)	93 (69 to 98)	99 (86 to 100)	100 (88 to 100)
Melanocytic nevi	93 (72 to 98)	96 (77 to 99)	94 (79 to 98)	99 (84 to 100)
SK	87 (58 to 94)	93 (64 to 99)	96 (83 to 99)	100 (89 to 100)

Note: BCC, basal cell carcinoma; CI, confidence interval; SK, seborrheic keratosis.

<sup>a</sup>Two criteria with the highest sensitivity and specificity.

Besides the specified features well consistent with classic histopathologic characteristics, HGM can provide information other than conventional H&E-stained pathologic examinations. During the examination of BCCs, many elongated cells with long dendritic processes were found in BCC nests through THG images. Similar findings have been reported in pigmented BCCs by reflectance confocal microscopy.<sup>40,41</sup> Immunohistochemical studies have shown that the dendritic cells populating in BCCs represent benign intratumoral melanocytes or Langerhans cells.<sup>40,41</sup> A recent publication has demonstrated that Langerhans cells and melanocytes share similar morphologic features as bright dendritic cells under *in vivo* reflectance confocal microscopy.<sup>42</sup> Our preliminary immunohistochemical studies also revealed CD1a- or HMB45-positive dendritic cells in the BCC nests.

We found that a better diagnostic performance by general assessment was achieved by analyzing the *ex vivo* data (99% sensitivity) in comparison with the *in vivo* data (92% sensitivity). The most important reason was that a better image quality could be obtained during *ex vivo* measurement without motion artifacts. In our study, it usually took ~5 to 10 min to acquire an HGM image stack. The time consumed increased if multiple sampling was required due to the size or heterogeneity of the tumor, or if adjustment of patient or instrument position due to difficult-to-reach skin areas with surface irregularities was required. Muscular fatigue or instability could cause image blurring or distortion after prolonged examination. For future clinical application in tumor screening, it will be more feasible to improve the speed of image acquisition.

In this study, HGM images could not be obtained from five lesions due to an overlying thick horny layer or being located on areas with irregular curvature where our objective lens could not be closely attached. A current existing limitation to HGM or to other noninvasive *in vivo* imaging technology is that it is difficult to assess tumors located on palms and soles with an overlying thick stratum corneum/stratum lucidum, or tumors covered with hyperkeratotic layers. The thick horny layers prevent infrared light penetration to the viable epidermis and dermis.<sup>18,37</sup> As most melanomas in Asians belong to acral lentiginous melanoma developing on palms and soles, the diagnosis of most melanomas in our patients by HGM was hampered. This might be improved by pretreatment with keratolytic agents on the lesions or testing of different immersion media to improve laser penetration.

In summary, our clinical trials support the evidence that *in vivo* HGM not only provides critical diagnostic information with a resolution comparable to traditional histopathology, but

also explicitly diagnoses skin diseases in nonmelanoma pigmented tumors. These advantages are important for clinicians to immediately access useful and reliable pathological information in the lesional sites for their diagnostic decisions. Due to the *in vivo* noninvasive imaging capability, HGM holds a great potential as a new modality for disease screening, diagnosis, classification, and continuous therapeutic monitoring during and after treatment.

### Acknowledgments

This project was supported by grants from National Health Research Institute (NHRI-EX102-9936EI), National Science Council (NSC 102-3011-P-002-010), and Molecular Imaging Center, National Taiwan University (MIC-1, 103R891601).

### References

1. P. Casson, "Basal cell carcinoma," *Clin. Plast. Surg.* **7**(3), 301–311 (1980).
2. S. Panda, "Nonmelanoma skin cancer in India: current scenario," *Indian J. Dermatol.* **55**(4), 373–378 (2010).
3. N. R. Telfer, G. B. Colver, and C. A. Morton, "Guidelines for the management of basal cell carcinoma," *Br. J. Dermatol.* **159**(1), 35–48 (2008).
4. J. M. Grant-Kels, E. T. Bason, and C. M. Grin, "The misdiagnosis of malignant melanoma," *J. Am. Acad. Dermatol.* **40**(4), 539–548 (1999).
5. R. Betti et al., "Seborrheic keratosis with compound nevus, junctional nevus and basal cell carcinoma in the same lesion," *Dermatology* **203**(3), 265–267 (2001).
6. M. Swerdlow, "Nevi; a problem of misdiagnosis," *Am. J. Clin. Pathol.* **22**(11), 1054–1060 (1952).
7. H. Pehamberger, A. Steiner, and K. Wolff, "In vivo epiluminescence microscopy of pigmented skin tumors. I. Pattern analysis of pigmented skin lesions," *J. Am. Acad. Dermatol.* **17**(4), 571–583 (1987).
8. R. O. Kenet et al., "Clinical diagnosis of pigmented lesions using digital epiluminescence microscopy: grading protocol and atlas," *Arch. Dermatol.* **129**(2), 157–174 (1993).
9. K. Terstappen, O. Larkö, and A. M. Wennberg, "Pigmented basal cell carcinoma—comparing the diagnostic methods of SIAscopy and dermoscopy," *Acta. Derm. Venereol.* **87**(3), 238–242 (2007).
10. C. C. Harland et al., "Differentiation of common benign pigmented skin lesions from melanoma by high-resolution ultrasound," *Br. J. Dermatol.* **143**(2), 281–289 (2000).
11. J. Welzel, "Optical coherence tomography in dermatology: a review," *Skin Res. Technol.* **7**(1), 1–9 (2001).
12. R. G. Langley et al., "Confocal scanning laser microscopy of benign and malignant melanocytic skin lesions in vivo," *J. Am. Acad. Dermatol.* **45**(3), 365–376 (2001).
13. K. J. Busam et al., "Morphologic features of melanocytes, pigmented keratinocytes, and melanophages by in vivo confocal scanning laser microscopy," *Mod. Pathol.* **14**(9), 862–868 (2001).

14. A. Gerger et al., "Diagnostic applicability of in vivo confocal laser scanning microscopy in melanocytic skin tumors," *J. Invest. Dermatol.* **124**(3), 493–498 (2005).
15. A. Gerger et al., "In vivo confocal laser scanning microscopy in the diagnosis of melanocytic skin tumours," *Br. J. Dermatol.* **160**(3), 475–481 (2009).
16. J. Paoli et al., "Multiphoton laser scanning microscopy on non-melanoma skin cancer: morphologic features for future non-invasive diagnostics," *J. Invest. Dermatol.* **128**(5), 1248–1255 (2008).
17. E. Dimitrow et al., "Sensitivity and specificity of multiphoton laser microscopy for in vivo and ex vivo diagnosis of malignant melanoma," *J. Invest. Dermatol.* **129**(7), 1752–1758 (2009).
18. J. Paoli, M. Smedh, and M. B. Ericson, "Multiphoton laser scanning microscopy—a novel diagnostic method for superficial skin cancers," *Semin. Cutan. Med. Surg.* **28**(3), 190–195 (2009).
19. S.-Y. Chen et al., "In vivo virtual biopsy of human skin by using non-invasive higher harmonic generation microscopy," *IEEE J. Sel. Topics Quantum Electron.* **16**(3), 478–492 (2010).
20. K. König and I. Riemann, "High-resolution multiphoton multimodal nonlinear spectral tomography of human skin with subcellular spatial resolution and picosecond time resolution," *J. Biomed. Opt.* **8**(3), 432–439 (2003).
21. K. König et al., "Clinical two-photon microendoscopy," *Microsc. Res. Tech.* **70**(5), 398–402 (2007).
22. K. König, "Clinical multiphoton tomography," *J. Biophotonics* **1**(1), 13–23 (2008).
23. C.-K. Sun et al., "Multiharmonic generation biopsy of skin," *Opt. Lett.* **28**(24), 2488–2490 (2003).
24. S.-W. Chu et al., "In vivo developmental biology study using noninvasive multi-harmonic generation microscopy," *Opt. Express* **11**(23), 3093–3099 (2003).
25. C.-K. Sun et al., "Higher harmonic generation microscopy for developmental biology," *J. Struct. Biol.* **147**(1), 19–30 (2004).
26. T. Yasui et al., "Ex vivo and in vivo second-harmonic-generation imaging of dermal collagen fiber in skin: comparison of imaging characteristics between mode-locked Cr:forsterite and Ti:sapphire lasers," *Appl. Opt.* **48**(10), D88–D95 (2009).
27. C.-S. Hsieh et al., "Higher harmonic generation microscopy of in vitro cultured mammal oocytes and embryos," *Opt. Express* **16**(15), 11574–11588 (2008).
28. K. König et al., "Cellular response to near-infrared femtosecond laser pulses in two-photon microscopes," *Opt. Lett.* **22**(2), 135–136 (1997).
29. O. Nadiarnykh et al., "Carcinogenic damage to deoxyribonucleic acid is induced by near-infrared laser pulses in multiphoton microscopy via combination of two- and three-photon absorption," *J. Biomed. Opt.* **17**(11), 116024 (2012).
30. S.-Y. Chen, H.-Y. Wu, and C.-K. Sun, "In vivo harmonic generation biopsy of human skin," *J. Biomed. Opt.* **14**(6), 060505 (2009).
31. Y.-H. Liao et al., "Determination of chronological aging parameters in epidermal keratinocytes by in vivo harmonic generation microscopy," *Biomed. Opt. Express* **4**(1), 77–88 (2013).
32. M.-R. Tsai et al., "Characterization of oral squamous cell carcinoma based on higher-harmonic generation microscopy," *J. Biophotonics* **5**(5–6), 415–424 (2012).
33. B. E. Bouma et al., "Self-phase-modulated Kerr-lens mode-locked Cr:forsterite laser source for optical coherence microscopy," *Opt. Lett.* **21**(22), 1839–1841 (1996).
34. S.-W. Chu et al., "Multimodal nonlinear spectral microscopy based on a femtosecond Cr:forsterite laser," *Opt. Lett.* **26**(23), 1909–1911 (2001).
35. J.-H. Lee et al., "Noninvasive in vivo assessment of epidermal hyperkeratosis and dermal fibrosis in atopic dermatitis," *J. Biomed. Opt.* **14**(1), 014008 (2009).
36. M.-R. Tsai et al., "In vivo optical virtual biopsy of human oral mucosa with harmonic generation microscopy," *Biomed. Opt. Express* **2**(8), 2317–2328 (2011).
37. R. Hofmann-Wellenhof et al., "Reflectance confocal microscopy—state-of-art and research overview," *Semin. Cutan. Med. Surg.* **28**(3), 172–179 (2009).
38. F. Fischer et al., "Risk estimation of skin damage due to ultrashort pulsed, focused near-infrared laser irradiation at 800 nm," *J. Biomed. Opt.* **13**(4), 041320 (2008).
39. B. R. Masters et al., "Mitigating thermal mechanical damage potential during two-photon dermal imaging," *J. Biomed. Opt.* **9**(6), 1265–1270 (2004).
40. S. Segura et al., "Dendritic cells in pigmented basal cell carcinoma: a relevant finding by reflectance-mode confocal microscopy," *Arch. Dermatol.* **143**(7), 883–886 (2007).
41. A. L. Agero et al., "Reflectance confocal microscopy of pigmented basal cell carcinoma," *J. Am. Acad. Dermatol.* **54**(4), 638–643 (2006).
42. P. Hashemi et al., "Langerhans cells and melanocytes share similar morphologic features under in vivo reflectance confocal microscopy: a challenge for melanoma diagnosis," *J. Am. Acad. Dermatol.* **66**(3), 452–462 (2012).

**Ming-Rung Tsai** received her PhD degree from the Graduate Institute of Photonics and Optoelectronics of National Taiwan University in 2013. Currently she is working as a postdoc at Molecular Imaging Center of National Taiwan University. Her major interests include biomedical imaging and image analysis.

**Yu-Hsiang Cheng** received the BS degree in electrical engineering and physics in 2011 and the MS degree in optoelectronics in 2013, both from National Taiwan University. His major interests include ultrafast laser optics and nonlinear microscopy.

**Jau-Shiuh Chen** is an attending physician in the dermatology department of National Taiwan University Hospital. The fields of his interest include cutaneous oncology, dermatologic surgery, and laser surgery. He currently chairs the executive committee of the Laser and Photonics Medicine Society of the R.O.C.

**Yi-Shuan Sheen** is an instructor of the Department of Dermatology, College of Medicine, National Taiwan University, Taiwan. She received the MD degree from Kaohsiung Medical University College of Medicine in 2004, and an MS degree from the Graduate Institute of Clinical Medicine, National Taiwan University, in 2009. Her research interests include melanoma, cutaneous carcinogenesis, dermatologic surgery and lasers.

**Yi-Hua Liao** is an assistant professor of the Department of Dermatology, College of Medicine, National Taiwan University, Taiwan. She received the MD degree from National Taiwan University College of Medicine in 1996, and a PhD degree from the Graduate Institute of Pathology, National Taiwan University, in 2007. Her research interests include melanoma, cutaneous carcinogenesis, dermatologic surgery and laser. She is currently the council member of the Laser and Photonics Medicine Society of the Republic of China and associate editor of *Dermatologica Sinica*.

**Chi-Kuang Sun** received his PhD degree in applied physics from Harvard University in 1995, and was an assistant researcher in the UCSB QUEST Center, from 1995 to 1996. In 1996, he joined National Taiwan University, where he is now a distinguished professor of photonics and optoelectronics and the chief director of Molecular Imaging Center. His research focuses on nano-acoustics, femtosecond optics, THz optoelectronics, and biomedical imaging. He is a fellow of OSA, SPIE, and IEEE.